

Enhancing Wireless Capsule Endoscopic Image Classification using Mayfly Algorithm with Deep Learning Approach

M. Amirthalingam¹, R. Ponnusamy²

¹Research Scholar, Department of Computer and Information Science, Annamalai University, Annamalai Nagar
Corresponding Author Email: [amir.cdm\[at\]gmail.com](mailto:amir.cdm[at]gmail.com)

²Assistant Professor, Department of Computer and Information Science, Annamalai University, Annamalai Nagar
Email: [povi2006\[at\]gmail.com](mailto:povi2006[at]gmail.com)

Abstract: *Wireless capsule endoscopy (WCE) image classification is a pivotal application of medical image analysis that mainly focuses on the automatic classification of images obtained by small ingestible capsules as they traverse the gastrointestinal tract. These images play a major role in the diagnosis and monitoring of different gastrointestinal disorders, namely small bowel tumors, inflammatory bowel disease, and gastrointestinal bleeding. Innovative machine learning (ML) and deep learning (DL) models are employed to categorize these images into applicable clinical categories, aiding healthcare professionals in making timely and accurate diagnoses. The development of robust classification approaches for WCE images has the potential to considerably improve the accuracy and efficiency of gastrointestinal disease detection, ultimately enhancing patient care and outcomes. This research introduces an Enhanced Wireless Capsule Endoscopic Image Classification employing Mayfly Algorithm with Deep Learning (WCEIC-MFADL) Approach. The major intention of WCEIC-MFADL technique focuses on classification and recognition of WCE images. To obtain this, WCEIC-MFADL technique follows a Gaussian filtering (GF) based noise removal procedure. Additionally, WCEIC-MFADL model uses SqueezeNet model for deriving feature vectors. For WCE image classification, the WCEIC-MFADL technique uses gated recurrent unit (GRU) model. At last, the MFA can be applied for the optimal hyperparameter tuning of the GRU model which aids in enhanced classifier results. To highlight improved performance of WCEIC-MFADL method, a huge range of simulations was involved. An experimental result stated that WCEIC-MFADL technique achieves better performance than other methods.*

Keywords: Wireless Capsule Endoscopy; Gastrointestinal Tract; Machine Learning; Gated Recurrent Unit; Image Classification

1. Introduction

Wireless capsule endoscopy (WCE) is a non-invasive method that measures substantially to offer diagnostic images of the small intestine [1]. In the WCE method, the patient swallows a capsule comprising a camera-embedded device that penetrates gastrointestinal (GI) tract and takes images as well as sends these captured images to an exterior receiver. Beginning in 1989 by a research team, the WCE technology has several developments over time by different businesses to become highly proficient and accurate, as we know it nowadays [2]. This technology changed the traditional endoscopy technique as well as made the analysis simpler for both investigator and patient due to standard endoscopy can be extremely troublesome and painful for patients [3]. In the WCE method, a camera takes images constantly for 8 hours inside the patients and transfers these images to the receiver, around 60000 images. A medical specialist analyses these images to identify which frames or images comprise the diseases or infections [4]. Due to massive quantity of images, it takes a considerable period for a healthcare professional to examine these images and it leads to an additional strain for physicians and causes poorer diagnosis of diseased regions of intestine [5]. Therefore, image recognition comprising infected areas employing diverse statistical and machine learning (ML) approaches has been an interesting research domain in recent decades [6]. An automatic identification system carries out an examination of the massive amount of images and determines the diseased images thus; it is simple for the

medical expert to analyze only those images, which contain visual contents of the impacted regions, and start proper corrective activities at a good time [7].

In recent years, artificial intelligence (AI) has established superior focus and deliberated by any of that a fourth industrial revolution. AI has a hierarchy of relations that covers ML and DL [8]. AI describes a computerized technique for resolving problems, which commonly want "human cognitive." ML has subcategories of AI that methods execute particular tasks without employing detailed commands. Alternatively, ML approach depends on implications and patterns [9]. DL has been described as a subtype of ML as well as mostly depends on deep artificial neural networks (DANNs). The key DL model for image analysis has convolutional neural networks (CNNs). The CNN model can be analogous to biological neurons in the human brain [10]. Particularly, it has been stimulated by the organization of the visual cortex⁹.

This research introduces an Enhanced Wireless Capsule Endoscopic Image Classification employing Mayfly Algorithm with Deep Learning (WCEIC-MFADL) Approach. A major intention of the WCEIC-MFADL technique focuses on classification and recognition of WCE images. To obtain this, WCEIC-MFADL model follows a Gaussian filtering (GF) based noise removal process. In addition, the WCEIC-MFADL technique employs SqueezeNet model for deriving feature vectors. For WCE image classification, the WCEIC-MFADL technique uses gated recurrent unit (GRU) model. At last, the MFA can be

Volume 12 Issue 11, November 2023

www.ijsr.net

Licensed Under Creative Commons Attribution CC BY

applied for the optimal hyperparameter tuning of the GRU model which aids in enhanced classifier results. To highlight the enhanced performance of WCEIC-MFADL technique, a huge range of simulations were involved.

2. Related works

Padmavathi and Harikiran [11] introduced the identification and classification of WCE diseased images via DNN as well as employed a bleed image recognizer (BIR) to connect MobileNetV2 model for classifying WCE diseased images. In the open-level assessment, the BIR utilizes MobileNetV2 architecture for its lower computation power requirements afterwards, the output was transferred to CNN for additional processing. Next, Bi-LSTM along with an attention mechanism has been implemented to increase effectiveness of method. The hybrid attention Bi-LSTM model produces a highly accurate classification efficiency. In [12], an innovative computer-aided diagnosis (CAD) system to identify irregularities in WCE images was developed. Following a preprocessing stage, the authors remove these images from descriptor and provide a kernel extreme learning machine (ELM) for execution of classification method.

Dey et al. [13] projected to devise and improve a comprehensive multiclass CNN classification method that could be employed in CAD technique to diagnose different GI tract infections by examining images of WCE-GI tract with differing tract lining infections. CNN classification-related solution architecture containing image processing improvement methods, data augmentation techniques, and diverse network models were developed. In [14], a CNN-based framework such as RAT-CapsNet was presented that consistently implements regional data and attention

mechanisms for classifying irregularities in WCE video data. This introduced RAT-CapsNet includes 2 main pipelines Compression and Regional Correlative Pipelines.

Rani et al. [15] developed an innovative automated method for identification of bleeding in WCE images by ensembling 3 pre-trained CNNs namely InceptionResNetV2, ResNet152V2, and InceptionV3 to reduce the period required to analyze the huge image databases as well as improve the accuracy of the exploration. Initially, the features could be removed by employing transfer learning (TL) on these pre-trained CNNs. Next, Principal Component Analysis (PCA) was exploited to choose the best feature sets from removed feature sets. Lastly, the chosen features have been combined and delivered to the Support Vector Machine (SVM) for classifying WCE images into 2 types namely normal and bleeding. Lu [16] aimed to employ NN rather than simulated endoscopic image diagnosis to support medical specialists in analyzing and handling endoscopic images. Initially, at image preprocessing, images are converted from RGB color into lab color modes, texture features are removed in network training and lastly, accurateness of method must be validated.

3. The proposed method

In this study paper, we present an enhanced WCEIC-MFADL approach. The major intention of the WCEIC-MFADL technique focuses on the recognition and classification of WCE images. The WCEIC-MFADL model includes GF-based pre-processing, SqueezeNet-based feature extraction, GRU-based classification, and MFA-based hyperparameter. Fig. 1 represents the workflow of WCEIC-MFADL approach.

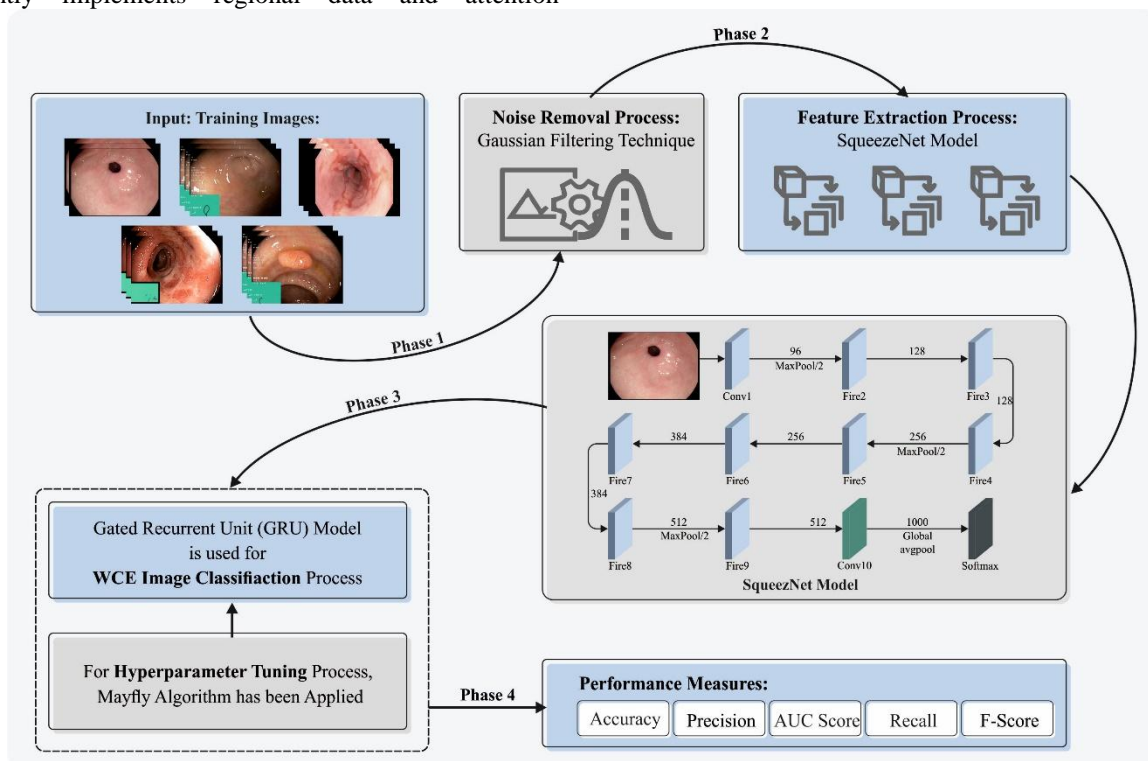


Figure 1: Workflow of WCEIC-MFADL approach

3.1 Preprocessing

Initially, the WCEIC-MFADL technique follows GF based noise removal process. As a widely used noise removal technique in image processing, GF exploits a Gaussian kernel to denoise and smooth images by averaging pixel values within a defined neighborhood [17]. GF diminishes high-frequency noise while maintaining structures and image details through the weighted average that prioritizes central pixel value. This method is especially useful for images overwhelmed by Gaussian-distributed noises, which contributes to high quality and clarity of images in different applications such as computer vision, photography, and medical imaging.

3.2 Feature extraction

At this stage, the WCEIC-MFADL technique employs SqueezeNet model for deriving feature vectors. SqueezeNet is a deep neural network (DNN) structure specifically engineered to overcome the problems of robust CNN on resource-constraint devices, such as embedded systems and mobile phones [18]. It was introduced to strike a balance among accuracy and model difficulty. The core technology in SqueezeNet is the usage of a "fire module," that considerably decreases the parameter number while preserving competitive accuracy. This includes a squeeze layer with 1x1 convolution to compress the input channel and the expanding layer which fuses combines 1x1 and 3x3 convolutions for capturing rigorous attributes. This diminishes model size, which makes it computation-effective and high memory.

The typical feature of SqueezeNet is its capability to preserve high performance on image classification benchmarks namely ImageNet, while applying a fraction of

parameter than difficult structures such as ResNet or VGG. This makes it a great solution for applications where computation efficiency and model size are crucial, especially in scenarios where real-time object detection, image classification, or other CV tasks are essential on devices with constrained computation abilities. The efficiency and effectiveness of Squeeze Net acts as a valuable tool in the field of DL, which offers an ideal solution to deploy deep CNN in a resource-constraint environment without compromising performance.

3.3 Classification using GRU model

For WCE image classification, the WCEIC-MFADL technique uses GRU model. GRU has good benefits in temporal data classification [19]. It extracts data from long-term sequences and prevents the gradient vanishing problem. Compared to LSTM, GRU has updated and reset gates that decrease the training time.

Reset gate forgets prior data and construct r_t . $r_t \in (0,1)$ is a scale factor which controls retention of prior state h_{t-1} . Update gate controls the effect of h_{t-1} and candidate \tilde{h}_t hidden layer on a hidden layer h_t , where z_t used to control the size of h_{t-1} and x_t in h_t :

$$r_t = \text{sigmoid}(\text{net}_r(t)) = \text{sigmoid}(W_{r_h}h_{t-1} + W_{r_x}x_t + b_r) \quad (1)$$

$$\tilde{h} = \tanh(\text{net}_{\tilde{h}}(t)) = \tanh(W_{\tilde{h}_x}x_t + W_{\tilde{h}_h}(r_t \odot h_{t-1}) + b_{\tilde{h}}) \quad (2)$$

$$z_t = \text{sigmoid}(\text{net}_z(t)) = \text{sigmoid}(W_{z_h}h_{t-1} + W_{z_x}x_t + b_z) \quad (3)$$

$$h_t = (1 - z_t)E \odot h_{t-1} + z_t \odot \tilde{h} \quad (4)$$

Where W_{*h} refers to weight among* and h_{t-1} , W_{*x} denotes weight between *and x_t , b_* is bias, while * can be \tilde{h} , r and z . Fig. 2 illustrates the framework of GRU model.

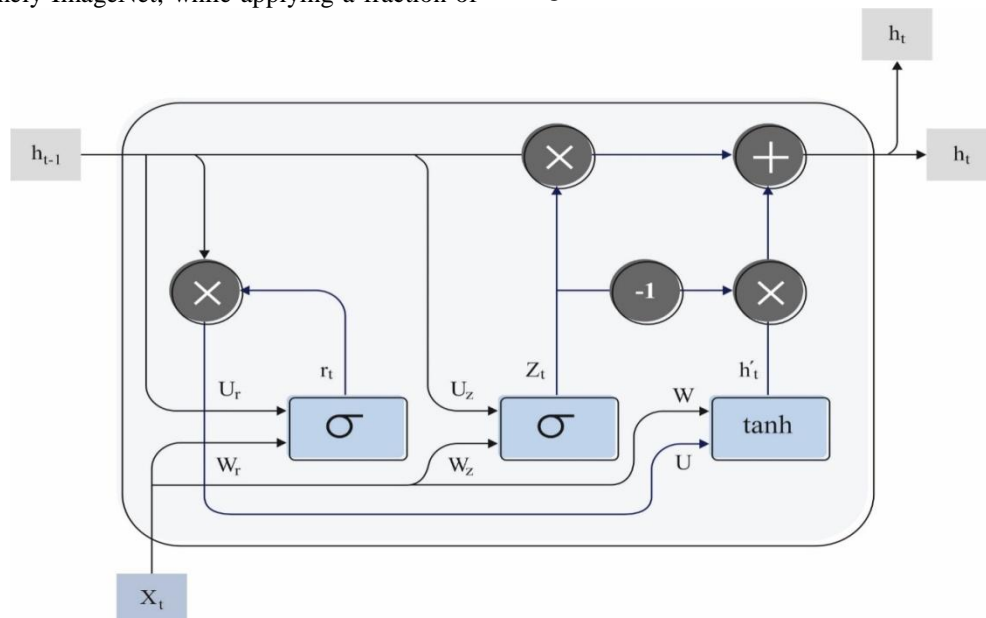


Figure 2: Architecture of GRU

3.4 MFA based hyperparameter tuning

At last, the MFA can be applied for the optimal hyperparameter tuning of the GRU model. MFA is one of the great techniques that developed depending on male mayfly's

(MMF) generative performance of appealing to females via dance [20]. This model merges benefits of FA and genetic algorithm (GA) on the base of PSO.

MFA search nearby in dual populations by upgrading their location and speed affording to exact guidelines. Male individuals modify their places when compared to each other. A male individual's location and speed are defined by Eqs. (5) and (6) correspondingly.

$$x_i^{k+1} = x_i^k + v_i^{k+1} \quad (5)$$

$$v_i^{k+1} = v_i^k + a_1 e^{-\beta r_p^2} (pbest_i - x_i^k) + a_2 e^{-\beta r_g^2} (gbest - x_i^k) \quad (6)$$

X_i^k denotes a position of MF i at k iteration; v_i^k states speed of MF i at k iteration; $pbest_i$ mentions optimal position that MF i ; a_1 and a_2 are positive attraction coefficient; r_p states Cartesian distance among MFs and individual's optimum position.

Females fly to raise as well as simplify mating device, best female allocated to optimal male, etc. so that female mayflies (FMF) speed and location calculated below:

$$v_i^{k+1} = v_i^k + a_2 e^{-\beta r_{mf}^2} (x_i^k - y_i^k), f(y_i) > f(x_i) \quad (7)$$

$$v_i^{k+1} = v_i^k = fl * r, f(y_i) \leq f(x_i) \quad (8)$$

$$y_i^{k+1} = y_i^k + v_i^{k+1} \quad (9)$$

Whereas v_i^k signifies speed of FMF i at k step, y_i^k denotes a position of FMF i at k step, r_{mf} denotes to speed of FME from males, and then fl means random movement coefficient.

A fundamental of MA is mating procedure among female and male populations. Affording to the above-mentioned standard of male appealing females, a cross process is executed via position measure of dual populations. A crossover structure is displayed in Eqs. (10) and (11):

$$offspring1 = L * male + (1 - L) * female \quad (10)$$

$$offspring2 = L * female + (1 - L) * male \quad (11)$$

Where L mentions random value within an exact range; male denotes individual MMF; female denotes individual FMF; $offspring$ states offspring MF individuals.

Under principle of preserving population size constant, advanced generation population attains a superior fitness value that will substitute consistent flexibility of preceding generation population or it will stay. In this phase, objective function $f(x)$ must employed in order to estimate and pick target population. During process of MFA, individual MF rapidity is very simple to raise huge value making a technique ineffectual. Individuals with lesser speed aid algorithms unite therefore it is essential to fix zero initial speed as well as speed higher limit for born individuals.

$$v_{max} = rand * (x_{max} - x_{min}) \quad (12)$$

It will affect calculation as well as drop into local optimal if individual speed is too small. So, speed higher limit defined affording to individual position.

Though a speed higher limit is set, it is highly compulsory to decrease speed when required. So, gravity co-efficient g is parallel to inertia co-efficient in PSO.

A speed of MMF attained by exchanging gravity co-efficient into calculation:

$$v_i^{k+1} = g * v_i^k + a_1 e^{-\beta r_p^2} (pbest_i - x_i^k) + a_2 e^{-\beta r_g^2} (gbest - x_i^k) \quad (13)$$

Female individual speed:

$$v_i^{k+1} = \begin{cases} g * v_i^k + a_2 e^{-\beta r_{mf}^2} (x_i^k - x_i^k), f(y_i) > f(x_i) \\ g * v_i^k + fl * r, f(y_i) \leq f(x_i) \end{cases} \quad (14)$$

The arbitrary movement co-efficient of MF is useful to jump out of local optimum trick in optimizer procedure but due to its huge primary value, it will central MF to transfer near poor regions. Then, it is highly essential to regularly follow novel random movement co-efficient in iteration procedure in order to decrease it.

$$d_k = d_0 \delta^k, 0 < \delta < 1 \quad (15)$$

$$fl_k = fl_0 \delta^k, 0 < \delta < 1 \quad (16)$$

Presenting genetic mutation devices of progeny to handle with probable local optimum convergence. A change in offspring basis MF to move complete novel search region.

$$offspring_n = offspring_n + \sigma N_n(0,1) \quad (17)$$

Whereas, $N_n(0,1)$ denotes normal distribution of standard by mean and σ signifies standard deviation of normal distribution.

The fitness selection is a considerable factor that influences performance of MFA model. The hyperparameter selection procedure includes a solution encoding technique to estimate efficiency of candidate solutions. In this study work, MFA technique considers accurateness as main principle to design fitness functions which are measured below:

$$Fitness = \max(P) \quad (18)$$

$$P = \frac{TP}{TP + FP} \quad (19)$$

From above mentioned expression, TP and FP denote true positive and false positive values, respectively.

4. Result analysis

Performance validation of WCEIC-MFADL model tested by employing Kvasir dataset [21] involves 6,000 images as defined in Table 1, marked and proved by doctors of medical (experienced endoscopists). It includes 6 classes that display anatomical landmarks, pathological results, or endoscopic processes in GI tract, i.e., 1000 images for every class. The classes include zline, pylorus, cecum, esophagitis, polyps, and ulcerative colitis. The dataset contains images with dissimilar resolutions from 720x576 to 1920x1072 pixels and is prepared in a method where they are organized in distinct folders termed according to content.

Table 1 Details of dataset

| Class | No. of Images |
|--------------------|---------------|
| zline | 1000 |
| pylorus | 1000 |
| cecum | 1000 |
| esophagitis | 1000 |
| polyps | 1000 |
| ulcerative colitis | 1000 |
| Total Images | 6000 |

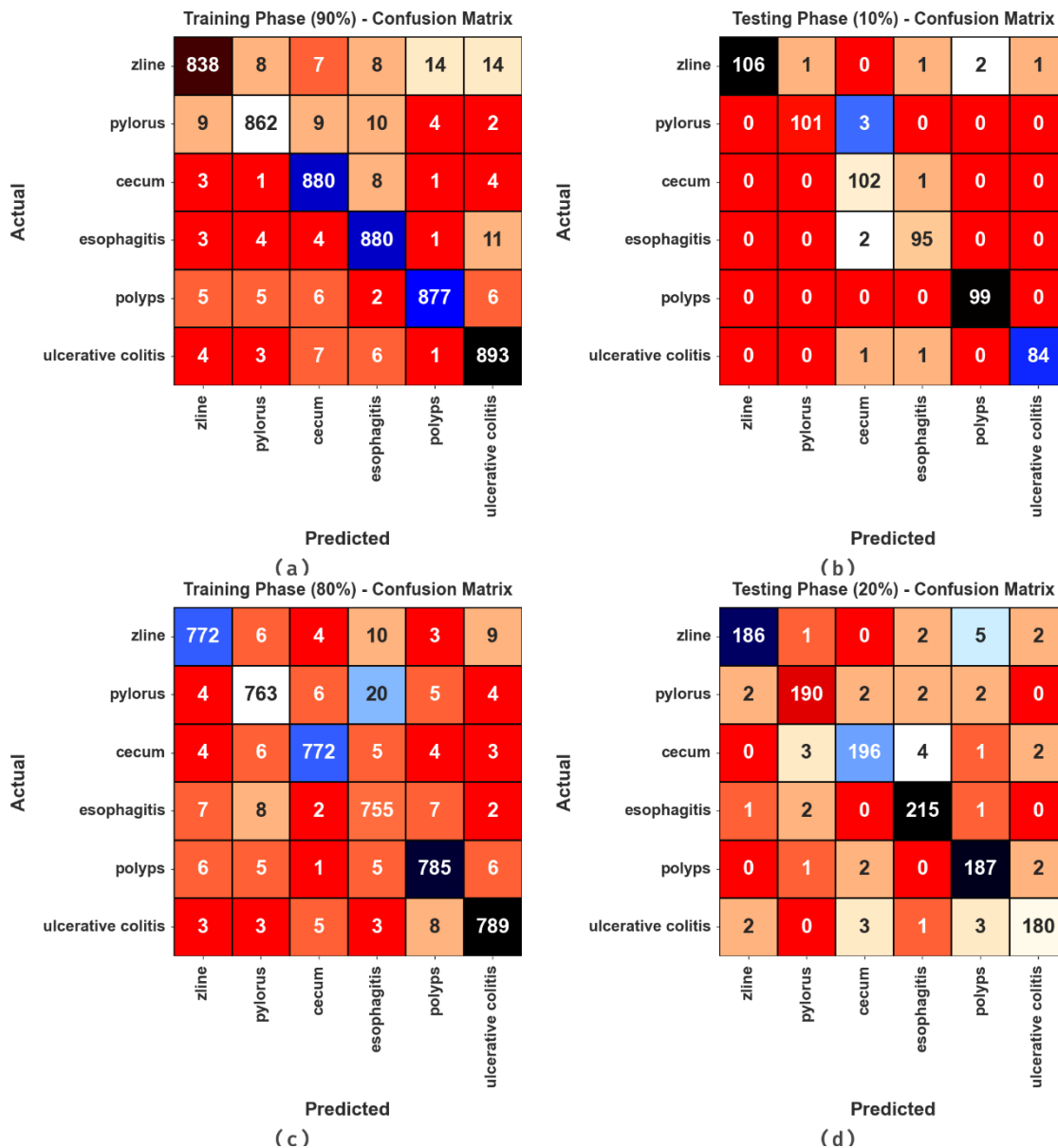


Figure 3: Confusion matrices of (a-c) TRPH of 90% and 80% and (b-d) TSPH of 10% and 20%

Fig. 3 establishes confusion matrices created by WCEIC-MFADL technique below 90:10 and 80:20 of TRPH/TSPH. The results specify effective detection and classification of all 6 classes.

The classification results of the WCEIC-MFADL technique are provided under 90:10 of TRPH/TSPH as defined in Table 2 and Fig. 4. The results showcase that WCEIC-

MFADL technique reaches enhanced performance. With 90% of TRPH, the WCEIC-MFADL technique offers average $accu_y$ of 98.95%, $prec_n$ of 96.86%, $reca_l$ of 96.84%, F_{score} of 96.85%, and AUC_{score} of 98.11%. Meanwhile, with 10% of TSPH, WCEIC-MFADL model provides average $accu_y$ of 99.28%, $prec_n$ of 97.87%, $reca_l$ of 97.88%, F_{score} of 97.85%, and AUC_{score} of 98.72%.

Table 2: Classifier outcome of WCEIC-MFADL technique on 90:10 of TRPH/TSPH

| Classes | $Accu_y$ | $Prec_n$ | $Reca_l$ | F_{Score} | AUC_{Score} |
|-----------------------------|--------------|--------------|--------------|--------------|---------------|
| Training Phase (90%) | | | | | |
| zline | 98.61 | 97.22 | 94.26 | 95.72 | 96.87 |
| pylorus | 98.98 | 97.62 | 96.21 | 96.91 | 97.87 |
| cecum | 99.07 | 96.39 | 98.10 | 97.24 | 98.69 |
| esophagitis | 98.94 | 96.28 | 97.45 | 96.86 | 98.35 |
| polyps | 99.17 | 97.66 | 97.34 | 97.50 | 98.43 |
| ulcerative colitis | 98.93 | 96.02 | 97.70 | 96.85 | 98.44 |
| Average | 98.95 | 96.86 | 96.84 | 96.85 | 98.11 |
| Testing Phase (10%) | | | | | |
| zline | 99.17 | 100.00 | 95.50 | 97.70 | 97.75 |
| pylorus | 99.33 | 99.02 | 97.12 | 98.06 | 98.46 |

| | | | | | |
|--------------------|--------------|--------------|--------------|--------------|--------------|
| cecum | 98.83 | 94.44 | 99.03 | 96.68 | 98.91 |
| esophagitis | 99.17 | 96.94 | 97.94 | 97.44 | 98.67 |
| polyps | 99.67 | 98.02 | 100.00 | 99.00 | 99.80 |
| ulcerative colitis | 99.50 | 98.82 | 97.67 | 98.25 | 98.74 |
| Average | 99.28 | 97.87 | 97.88 | 97.85 | 98.72 |

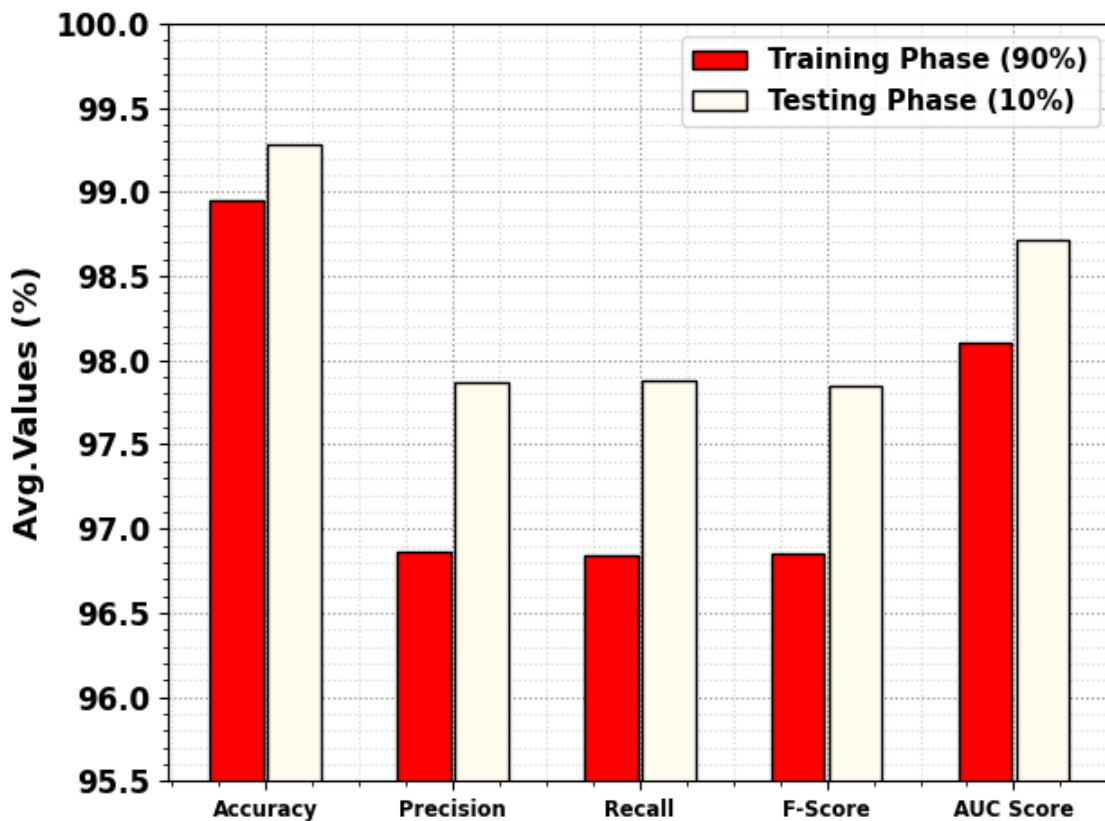


Figure 4: Average of WCEIC-MFADL technique on 90:10 of TRPH/TSPH Training and Validation Accuracy (90:10)

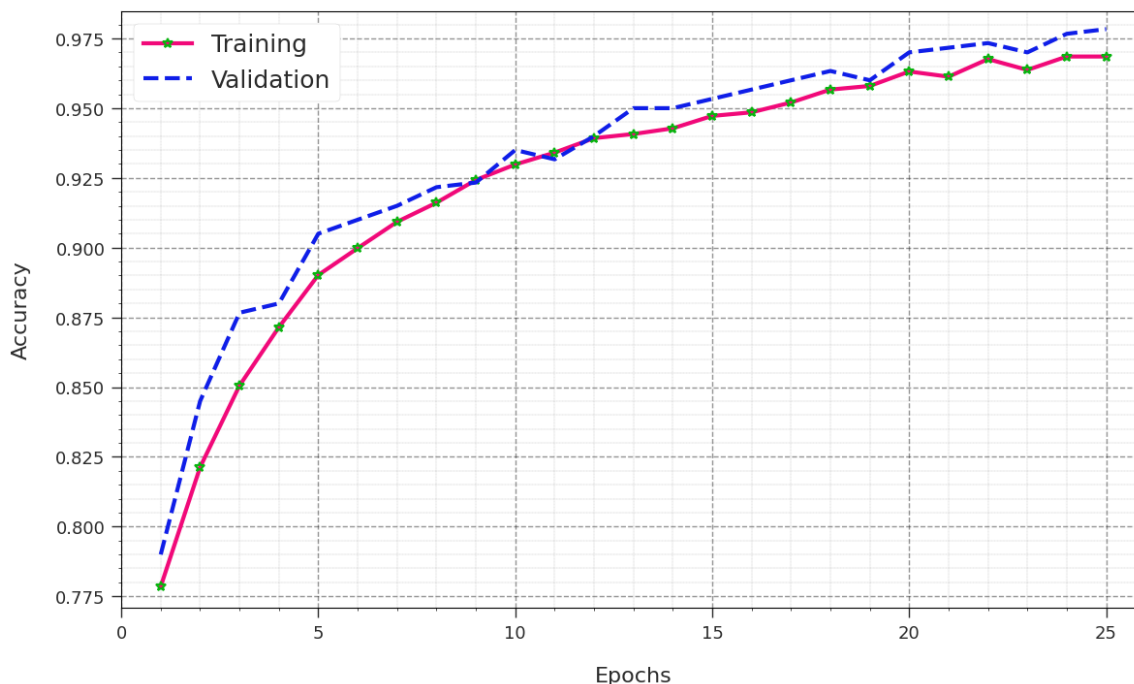


Figure 5: Accuracy curve of WCEIC-MFADL technique on 90:10 of TRPH/TSPH

The training and validation accurateness curves of WCEIC-MFADL model on 90:10 of TRPH/TSPH shown in Fig. 5 deliver respected insights into performance of WCEIC-MFADL technique over many epochs. These curves

underline crucial insights into learning procedure and model's ability to simplify. Additionally, it is noticeable that there is a consistence development in TR and TS accuracy over growing epochs. It highlighted model's ability to learn and identify patterns in both training and testing datasets. The increasing testing exactness recommends that the model adapts to training data as well as excels in creating precise forecasts on earlier unseen data, highlighting its robust generalization skills.

In Fig. 6, we signify a complete opinion of TR and TS loss values for WCEIC-MFADL technique on 90:10 of TRPH/TSPH through dissimilar epochs. TR loss gradually reduces model and enhances its weights to decrease classification errors on both TR and TS datasets. These loss curves offer a perfect image of how well the model supports training data, underscoring its aptitude to professionally grip patterns in both datasets. It is value noticeable that WCEIC-MFADL model constantly improves its parameters for reducing differences between prediction and actual training labels.

Training and Validation Loss (90:10)

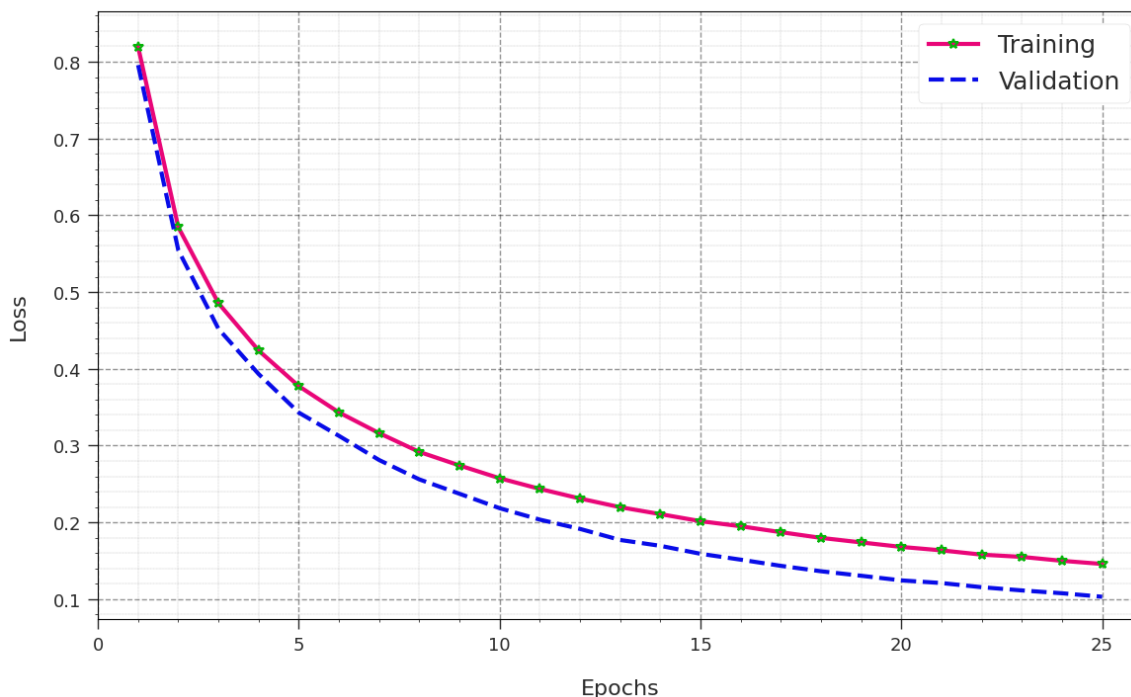


Figure 6: Loss curve of WCEIC-MFADL technique on 90:10 of TRPH/TSPH

Precision-Recall Curve (90:10)

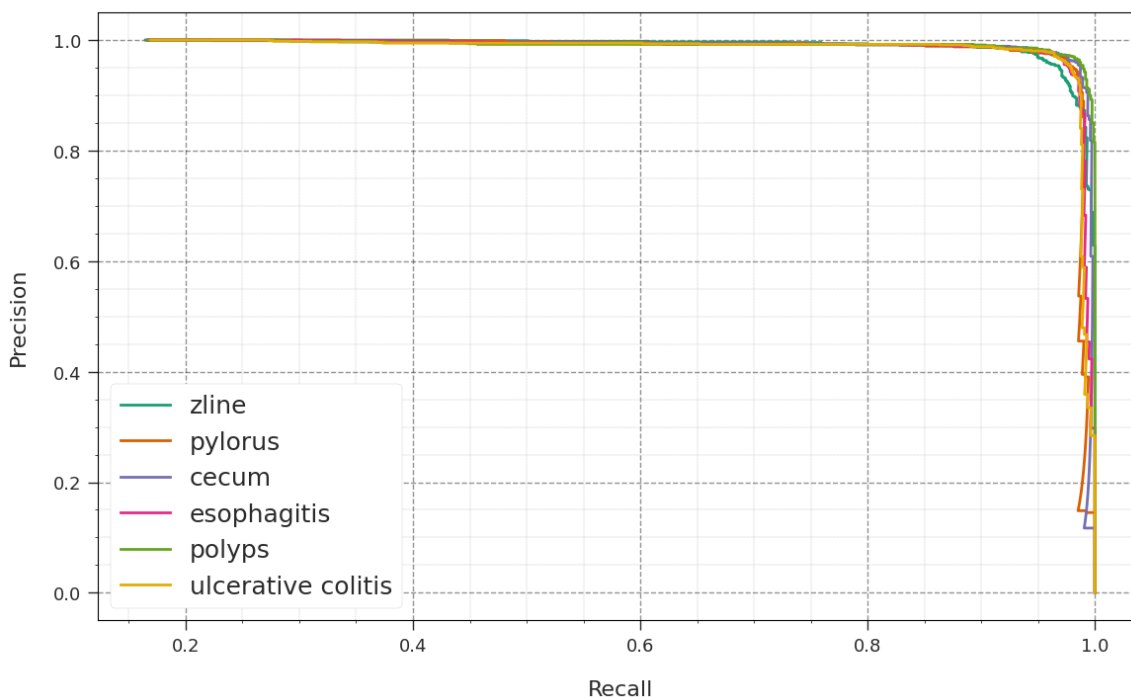


Figure 7: PR curve of WCEIC-MFADL technique on 90:10 of TRPH/TSPH

With respect to precision-recall curve as assumed in Fig. 7, the results visibly approve that WCEIC-MFADL technology on 90:10 of TRPH/TSPH increasingly achieves improved precision-recall values through each class. The outcomes highlight effective capability of model in discrimination of dissimilar classes, prominence efficiency in detection of class labels.

Besides, in Fig. 8, we present ROC curves formed by WCEIC-MFADL model on 90:10 of TRPH/TSPH, which excel in discriminating among classes. These curves offer respected insights into balance among TPR and FPR across disparate classification thresholds and epochs. The results highlight exact classification performance below diverse class labels, underlining performance in handling diverse classification tasks.

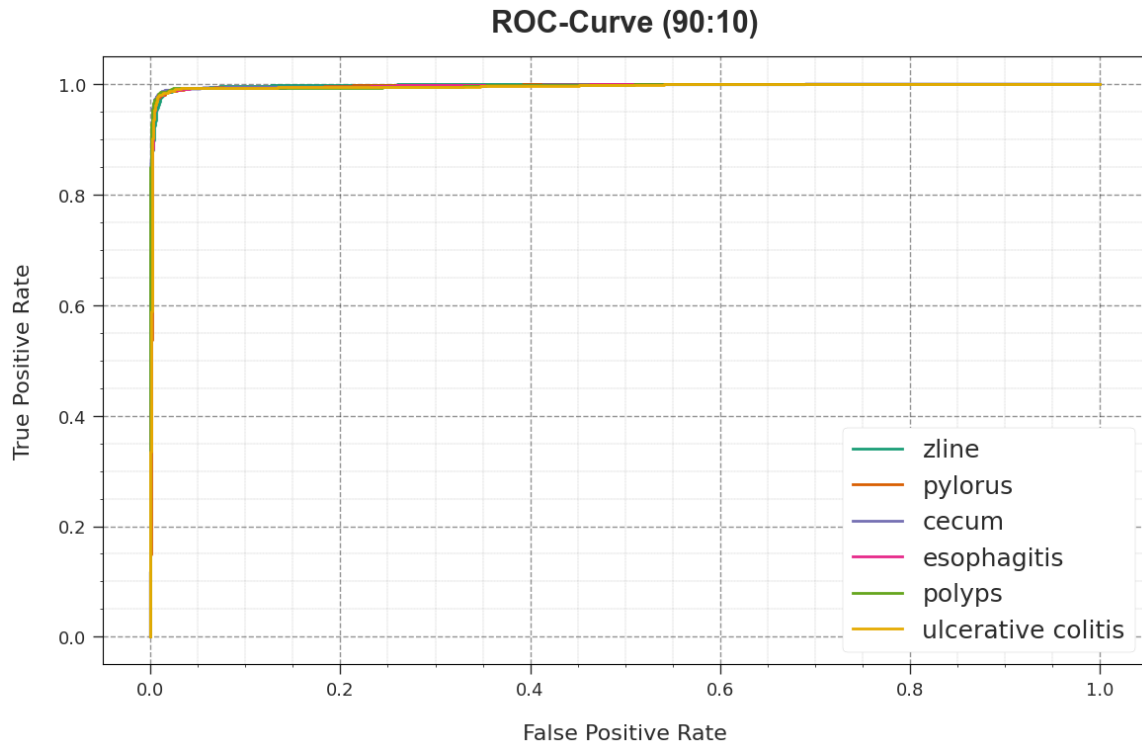


Figure 8: ROC curve of WCEIC-MFADL technique on 90:10 of TRPH/TSPH

The classification results of WCEIC-MFADL methodology delivered below 80:20 of TRPH/TSPH as denoted in Table 3 and Fig. 9. The results show that WCEIC-MFADL method extends improved performance. With 80% of TRPH, WCEIC-MFADL model provides average $accu_y$ of 98.86%, $prec_n$ of 96.58%, $reca_l$ of 96.58%, F_{score} of 96.58%, and AUC_{score} of 97.95%. Meanwhile, with 20% of TSPH, WCEIC-MFADL model provides average $accu_y$ of 98.72%, $prec_n$ of 96.18%, $reca_l$ of 96.14%, F_{score} of 96.15%, and AUC_{score} of 97.68%.

Table 3: Classifier outcome of WCEIC-MFADL technique on 80:20 of TRPH/TSPH

| Classes | $Accu_y$ | $Prec_n$ | $Reca_l$ | F_{score} | AUC_{score} |
|-----------------------------|--------------|--------------|--------------|--------------|---------------|
| Training Phase (80%) | | | | | |
| zline | 98.83 | 96.98 | 96.02 | 96.50 | 97.71 |
| pylorus | 98.60 | 96.46 | 95.14 | 95.79 | 97.22 |
| cecum | 99.17 | 97.72 | 97.23 | 97.47 | 98.39 |
| esophagitis | 98.56 | 94.61 | 96.67 | 95.63 | 97.80 |
| polyps | 98.96 | 96.67 | 97.15 | 96.91 | 98.24 |
| ulcerative colitis | 99.04 | 97.05 | 97.29 | 97.17 | 98.34 |
| Average | 98.86 | 96.58 | 96.58 | 96.58 | 97.95 |
| Testing Phase (20%) | | | | | |
| zline | 98.75 | 97.38 | 94.90 | 96.12 | 97.20 |
| pylorus | 98.75 | 96.45 | 95.96 | 96.20 | 97.63 |
| cecum | 98.58 | 96.55 | 95.15 | 95.84 | 97.22 |
| esophagitis | 98.92 | 95.98 | 98.17 | 97.07 | 98.63 |
| polyps | 98.58 | 93.97 | 97.40 | 95.65 | 98.10 |
| ulcerative colitis | 98.75 | 96.77 | 95.24 | 96.00 | 97.32 |
| Average | 98.72 | 96.18 | 96.14 | 96.15 | 97.68 |

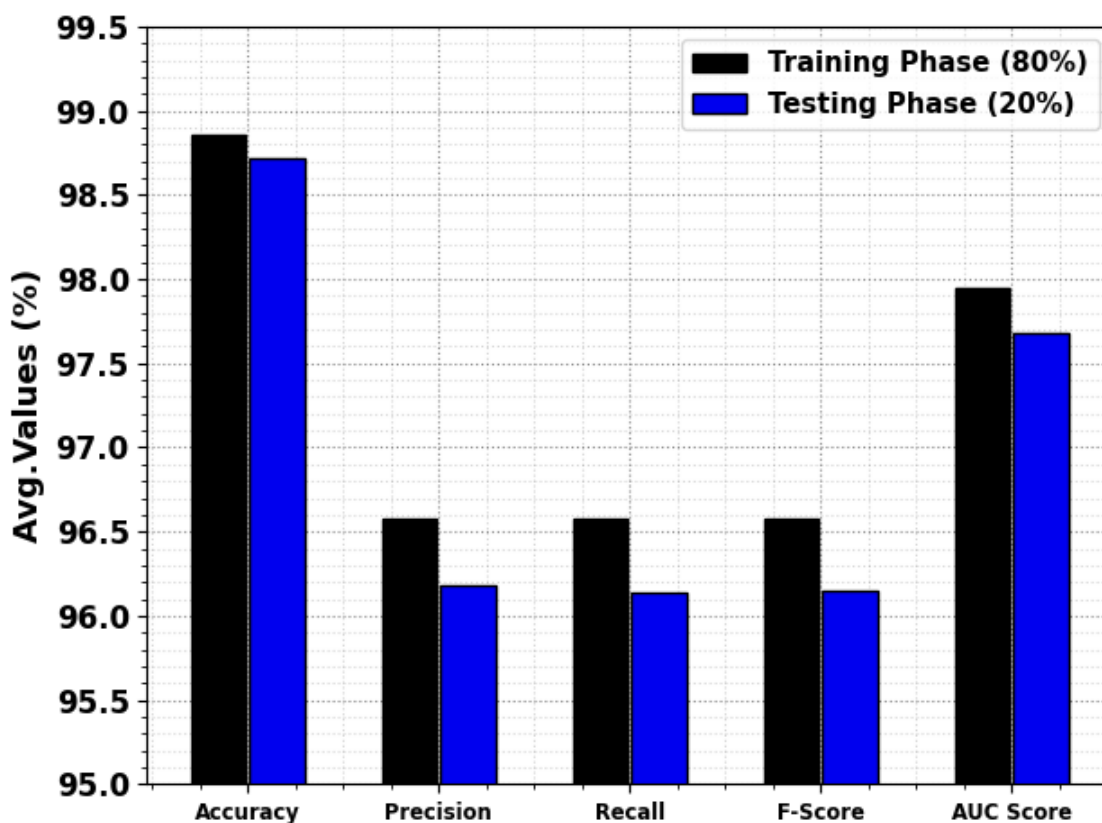


Figure 9: Average of WCEIC-MFADL technique on 80:20 of TRPH/TSPH Training and Validation Accuracy (80:20)

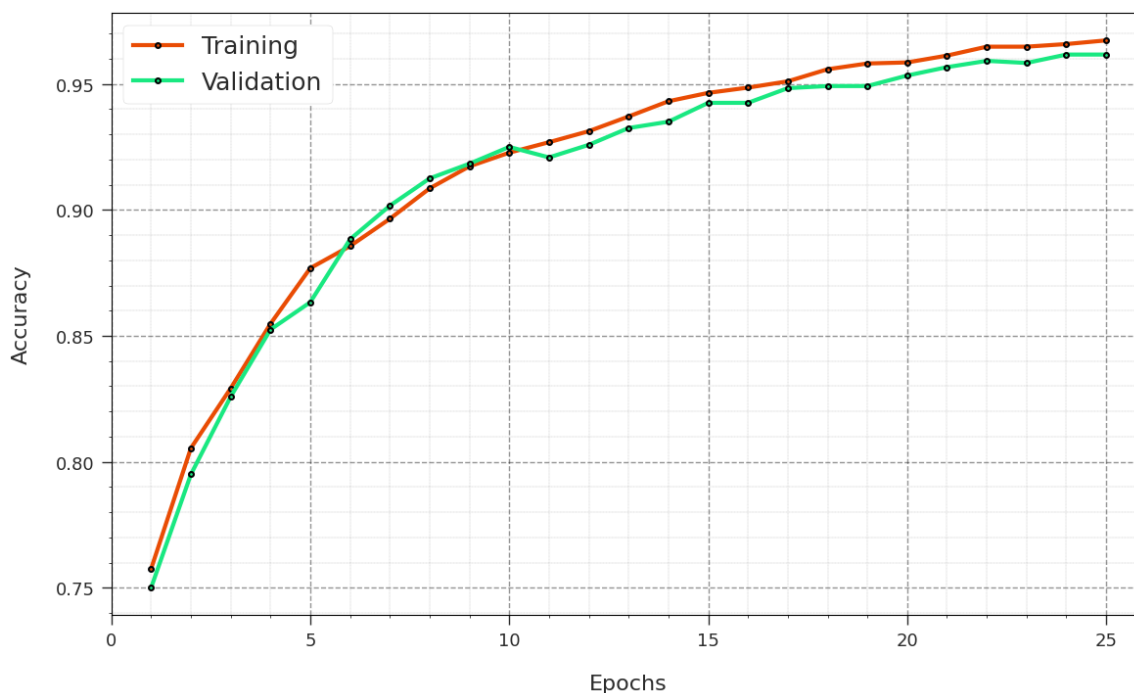


Figure 10: Accuracy curve of WCEIC-MFADL technique on 80:20 of TRPH/TSPH

The training and validation exactness curves of WCEIC-MFADL model on 80:20 of TRPH/TSPH displayed in Fig. 10, deliver treasured visions of the performance of WCEIC-MFADL technology over several epochs. These curves highlight vital insights into learning procedures and model's aptitude to simplify. In addition to that, it can be visible that there is a consistency enhancement in TR and TS exactness

over increasing epochs. It pointed out model's ability to learn and distinguish patterns within both training and testing datasets. The increasing testing exactness recommends that model not only familiarizes with training data but also shines in generating precise predictions on previously unseen data, highlighting its vigorous generalization skills.

In Fig. 11, we denote an inclusive opinion of TR and TS loss values for WCEIC-MFADL model on 80:20 of TRPH/TSPH across dissimilar epochs. TR loss gradually decreases as the model boosts its weights to diminish classification errors on both TR and TS datasets. These loss curves offer a clear picture of how well the method associates with training data,

emphasizing its power to competently influence patterns in both datasets. It is valuable to notice that the WCEIC-MFADL method constantly perfects its parameters for reducing divergences between prediction and real training labels.

Training and Validation Loss (80:20)

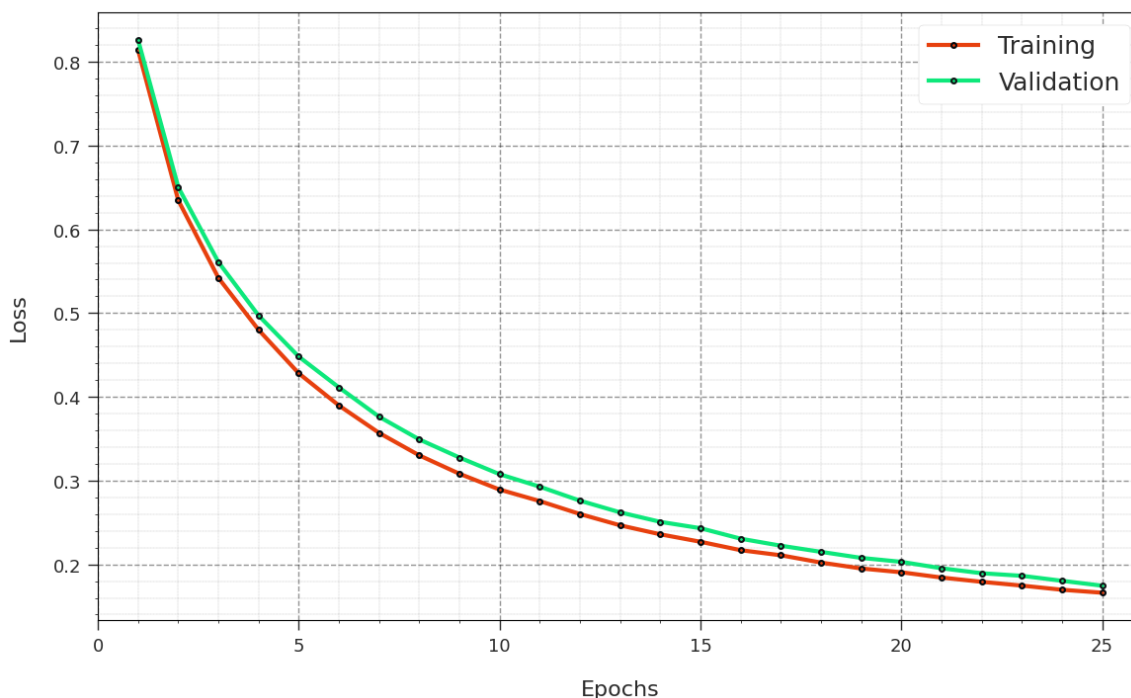


Figure 11: Loss curve of WCEIC-MFADL technique on 80:20 of TRPH/TSPH
Precision-Recall Curve (80:20)

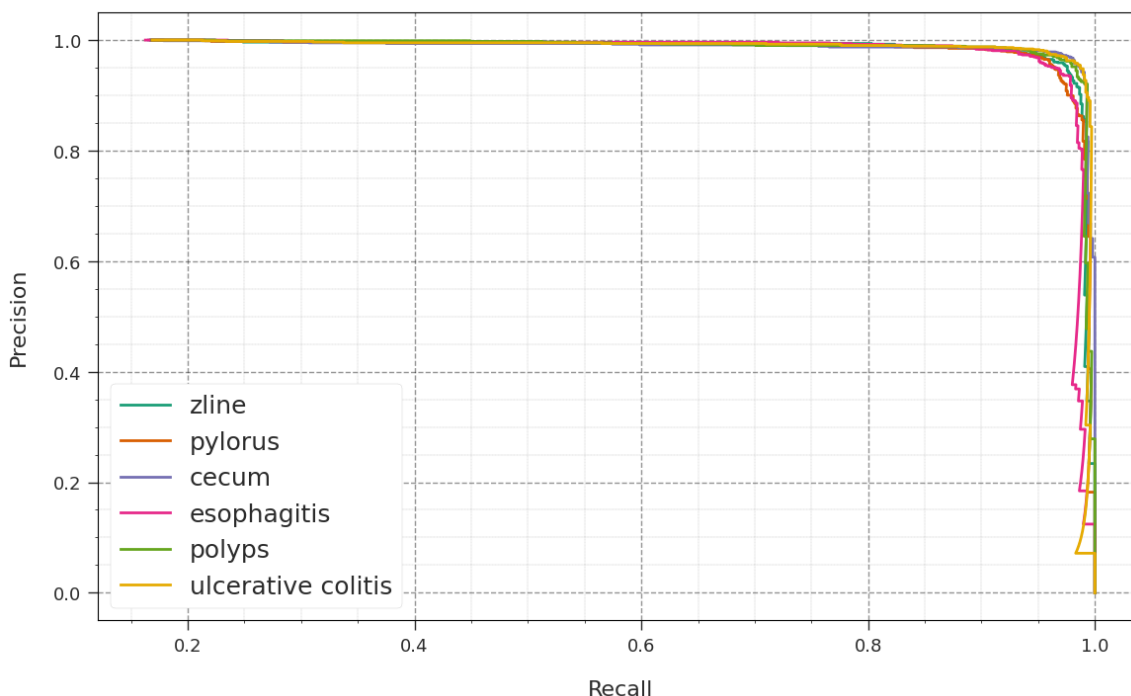


Figure 12: PR curve of WCEIC-MFADL technique on 80:20 of TRPH/TSPH

With esteem to precision-recall curve, as specified in Fig. 12, the outcomes obviously confirm that WCEIC-MFADL model on 80:20 of TRPH/TSPH gradually achieves improved precision-recall values through each class. The results focus effective capacity of model in perception of

dissimilar classes, underlining efficiency in classification of class labels.

Moreover, in Fig. 13, we establish ROC curves created by WCEIC-MFADL methodology on 80:20 of TRPH/TSPH,

which stand out in distinguishing amid classes. These curves deliver respected insights into balance among TPR and FPR through dissimilar classification thresholds and epochs. The

results highlight exact classification performance below diverse class labels, emphasizing performance in addressing various classification tasks.

ROC-Curve (80:20)

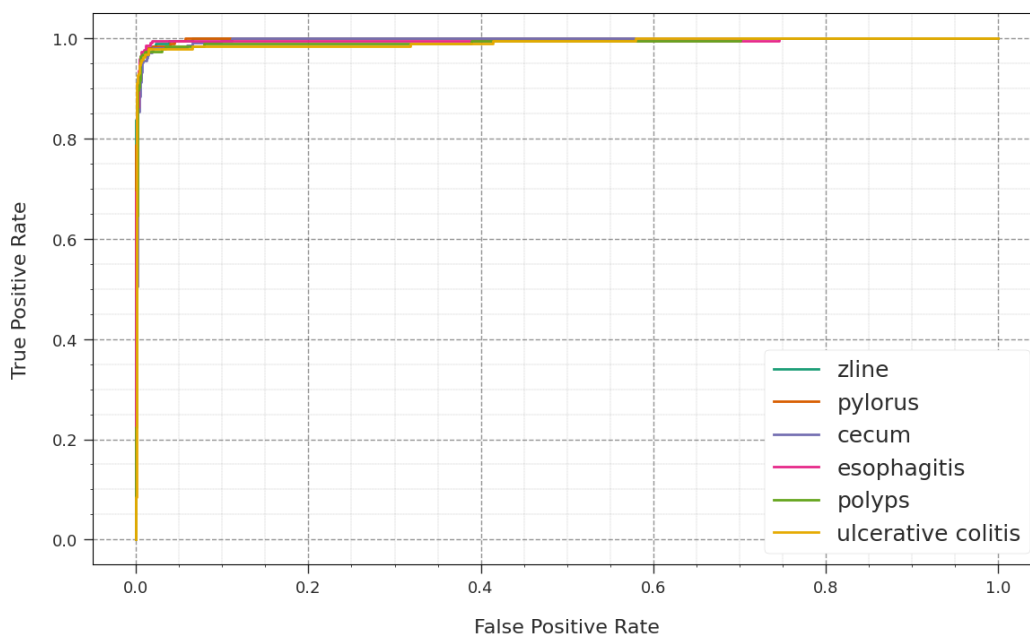


Figure 13: ROC curve of WCEIC-MFADL technique on 80:20 of TRPH/TSPH

In Table 4 and Fig. 14, a complete comparison study of WCEIC-MFADL technology is provided. The results designate that LR and SVM methods obtain poor performance whereas ETC and DTC models demonstrate slightly boosted results. Meanwhile, IWEIC-GOADL, WCEIC-RSADL, IWSO-DLIC, and WCEIC-SOADL models accomplish reasonable performance. However, the WCEIC-MFADL technique gains maximum performance with $accu_y$ of 99.28%, $prec_n$ of 97.87%, $reca_l$ of 97.88%, and $F1_{score}$ of 97.85%. Thus, the WCEIC-MFADL technique can be employed for accurate WCE image classification.

Table 4: Comparative outcome of WCEIC-MFADL technique with other existing approaches

| Methods | $Accu_y$ | $Prec_n$ | $Reca_l$ | $F1_{score}$ |
|-------------|----------|----------|----------|--------------|
| WCEIC-MFADL | 99.28 | 97.87 | 97.88 | 97.85 |
| IWEIC-GOADL | 99.13 | 99.21 | 99.13 | 99.16 |
| WCEIC-RSADL | 98.72 | 98.81 | 98.72 | 98.75 |
| IWSO-DLIC | 98.57 | 98.08 | 98.57 | 98.29 |
| WCEIC-SOADL | 97.78 | 97.78 | 97.78 | 97.78 |
| RF | 96.51 | 97.34 | 97.10 | 97.23 |
| ETC | 93.36 | 93.72 | 93.46 | 92.80 |
| LR | 87.46 | 90.50 | 88.49 | 88.36 |
| SVM | 89.31 | 91.08 | 88.78 | 88.77 |
| DTC | 90.60 | 92.57 | 91.62 | 91.06 |

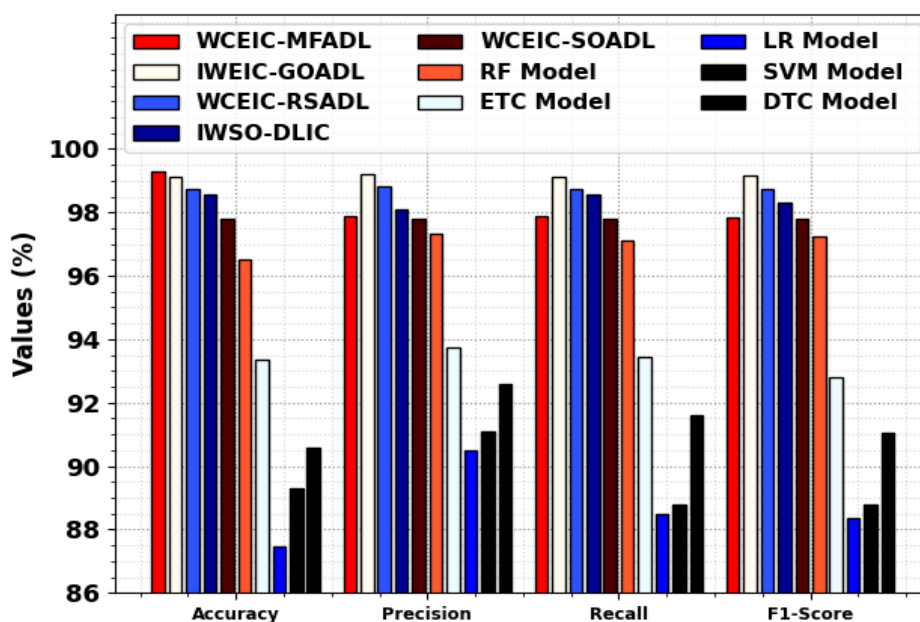


Figure 14: Comparative outcome of WCEIC-MFADL technique with other existing approaches

5. Conclusion

In this study, we introduce an enhanced WCEIC-MFADL approach. The major intention of the WCEIC-MFADL technique focuses on the recognition and classification of WCE images. The WCEIC-MFADL model includes GF-based preprocessing, SqueezeNet based feature extraction, GRU based classification, and MFA based hyperparameter. To obtain this, the WCEIC-MFADL technique follows GF based noise removal process and then employs SqueezeNet model for deriving feature vectors. Moreover, the WCEIC-MFADL technique uses GRU model. At last, the MFA can be applied for the optimal hyperparameter tuning of the GRU model which aids in enhanced classifier results. To highlight superior performance of WCEIC-MFADL model, a huge range of simulations is involved. An experimental result stated that the WCEIC-MFADL technique achieves better performance than other models.

References

- [1] Muhammad, K., Khan, S., Kumar, N., Del Ser, J. and Mirjalili, S., 2020. Vision-based personalized wireless capsule endoscopy for smart healthcare: taxonomy, literature review, opportunities and challenges. *Future Generation Computer Systems*, 113, pp.266-280.
- [2] Lafraxo, S. and El Ansari, M., 2020, October. GastroNet: Abnormalities Recognition in Gastrointestinal Tract through Endoscopic Imagery using Deep Learning Techniques. In *2020 8th International Conference on Wireless Networks and Mobile Communications (WINCOM)* (pp. 1-5). IEEE.
- [3] Shahril, R., Saito, A., Shimizu, A. and Baharun, S., 2020. Bleeding Classification of Enhanced Wireless Capsule Endoscopy Images using Deep Convolutional Neural Network. *Journal of Information Science & Engineering*, 36(1).
- [4] Bajhaiya, D. and Unni, S.N., 2022, April. Deep learning-enabled classification of gastric ulcers from wireless-capsule endoscopic images. In *Medical Imaging 2022: Digital and Computational Pathology* (Vol. 12039, pp. 352-356). SPIE.
- [5] Jain, S., Seal, A. and Ojha, A., 2021. Deep learning models for anomaly detection in wireless capsule endoscopy video frames: The transfer learning approach. In *Smart Computing* (pp. 423-432). CRC Press.
- [6] Bouyaya, D., Benierbah, S. and Khamadja, M., 2021. An intelligent compression system for wireless capsule endoscopy images. *Biomedical Signal Processing and Control*, 70, p.102929.
- [7] Muruganantham, P. and Balakrishnan, S.M., 2021. A survey on deep learning models for wireless capsule endoscopy image analysis. *International Journal of Cognitive Computing in Engineering*, 2, pp.83-92.
- [8] Khan, M.A., Kadry, S., Alhaisoni, M., Nam, Y., Zhang, Y., Rajinikanth, V. and Sarfraz, M.S., 2020. Computer-aided gastrointestinal diseases analysis from wireless capsule endoscopy: a framework of best features selection. *IEEE Access*, 8, pp.132850-132859.
- [9] Raut, V. and Gunjan, R., 2022. Transfer learning based video summarization in wireless capsule endoscopy. *International Journal of Information Technology*, pp.1-8.
- [10] Yin, T.K., Huang, K.L., Chiu, S.R., Yang, Y.Q. and Chang, B.R., 2022. Endoscopy Artefact Detection by Deep Transfer Learning of Baseline Models. *Journal of Digital Imaging*, pp.1-10.
- [11] Padmavathi, P. and Harikiran, J., 2023. Wireless Capsule Endoscopy Infected Images Detection and Classification Using MobileNetV2-BiLSTM Model. *International Journal of Image and Graphics*, 23(05), p.2350041.
- [12] Ellahyani, A., Jaafari, I.E., Charfi, S. and Ansari, M.E., 2021. Detection of abnormalities in wireless capsule endoscopy based on extreme learning machine. *Signal, Image and Video Processing*, 15, pp.877-884.
- [13] Dey, R.K., Rana, M.E. and Hameed, V.A., 2023, January. Analysing Wireless Capsule Endoscopy Images Using Deep Learning Frameworks to Classify Different GI Tract Diseases. In *2023 17th International Conference on Ubiquitous Information Management and Communication (IMCOM)* (pp. 1-7). IEEE.
- [14] Alam, M.J., Rashid, R.B., Fattah, S.A. and Saquib, M., 2022. RA-CapsNet: A Deep Learning Network Utilizing Attention and Regional Information for Abnormality Detection in Wireless Capsule Endoscopy. *IEEE Journal of Translational Engineering in Health and Medicine*, 10, pp.1-8.
- [15] Rani, K., Devi, G., Kumar, S., Figueiredo, I.N. and Figueiredo, P.N., 2022, November. Classification of wireless capsule endoscopy images for bleeding using deep features fusion. In *2022 International Conference on Electrical, Computer, Communications and Mechatronics Engineering (ICECCME)* (pp. 1-6). IEEE.
- [16] Lu, B., 2022. Image Aided Recognition of Wireless Capsule Endoscope Based on the Neural Network. *Journal of Healthcare Engineering*, 2022.
- [17] Nyemeesha, V. and Ismail, B.M., 2021. Implementation of noise and hair removals from dermoscopy images using hybrid Gaussian filter. *Network Modeling Analysis in Health Informatics and Bioinformatics*, 10, pp.1-10.
- [18] Rasool, M., Ismail, N.A., Al-Dhaqm, A., Yafouz, W.M. and Alsaedi, A., 2022. A Novel Approach for Classifying Brain Tumours Combining a SqueezeNet Model with SVM and Fine-Tuning. *Electronics*, 12(1), p.149.
- [19] Lei, X., Shilin, D., Shangqin, T., Changqiang, H., Kangsheng, D. and Zhuoran, Z., 2023. Beyond visual range maneuver intention recognition based on attention enhanced tuna swarm optimization parallel BiGRU. *Complex & Intelligent Systems*, pp.1-22.
- [20] Mo, S., Ye, Q., Jiang, K., Mo, X. and Shen, G., 2022. An improved MPPT method for photovoltaic systems based on mayfly optimization algorithm. *Energy Reports*, 8, pp.141-150.
- [21] Pogorelov, K., Randel, K.R., Griwodz, C., Eskeland, S.L., de Lange, T., Johansen, D., Spampinato, C., Dang-Nguyen, D.T., Lux, M., Schmidt, P.T. and Riegler, M., 2017, June. Kvasir: A multi-class image dataset for computer aided gastrointestinal disease detection. In *Proceedings of the 8th ACM on Multimedia Systems Conference* (pp. 164-169)